

Isotopic Scaling in Nuclear Reactions

M. B. Tsang,¹ W. A. Friedman,² C. K. Gelbke,¹ W. G. Lynch,¹ G. Verde,¹ and H. S. Xu¹

¹National Superconducting Cyclotron Laboratory and Department of Physics and Astronomy,
Michigan State University, East Lansing, Michigan 48824

²Department of Physics, University of Wisconsin, Madison, Wisconsin 53706

(Received 12 July 2000; revised manuscript received 16 February 2001)

A three parameter scaling relationship between isotopic distributions for elements with $Z \leq 8$ has been observed. This allows a simple description of the dependence of such distributions on the overall isospin of the system. This scaling law (termed isoscaling) applies for a variety of reaction mechanisms that are dominated by phase space, including evaporation, multifragmentation, and deeply inelastic scattering. The origins of this scaling behavior for the various reaction mechanisms are explained. For multifragmentation processes, the systematics is influenced by the density dependence of the asymmetry term of the equation of state.

DOI: 10.1103/PhysRevLett.86.5023

PACS numbers: 24.60.Ky, 24.10.Pa, 25.70.Pq

The availability of high intensity radioactive beams facilitates the exploration of the isospin degree of freedom in nuclear reactions. Understanding the connection between the entrance channel isospin and the isotopic distribution of reaction products is important for studying the charge asymmetry term of the nuclear equation-of-state [1–3], obtaining information about charge equilibration [4–6], providing stringent tests for reaction models, and optimizing the production of rare isotopes far from stability. In this Letter, we demonstrate that isotopic distributions for statistical production mechanisms follow scaling laws. We also find circumstances where the values for the scaling parameters are influenced by the density dependence of the asymmetry term of the nuclear equation of state, a quantity that influences many important properties of neutron stars.

The scaling laws in question relate ratios of isotope yields measured in two different nuclear reactions, 1 and 2, $R_{21}(N, Z) = Y_2(N, Z)/Y_1(N, Z)$. In multifragmentation events, such ratios were shown to obey an exponential dependence on the neutron and proton number of the isotopes characterized by three parameters α , β , and C [7]:

$$R_{21}(N, Z) = C \exp(\alpha N + \beta Z). \quad (1)$$

Here we choose the convention that the isospin composition (neutron to proton ratio) of system 2 is larger than that of system 1. The systematics described by Eq. (1) occur naturally within the grand-canonical ensemble [7–9]. As shown in Ref. [7], the parameters α and β in that limit are the differences between the neutron and proton chemical potentials for the two reactions (i.e., $\alpha = \Delta\mu_n/T$ and $\beta = \Delta\mu_p/T$), and C is an overall normalization constant.

The accuracy of the isoscaling described by Eq. (1) can be compactly displayed if one plots the scaled isotopic ratio,

$$S(N) = R_{21}(N, Z) \exp(-\beta Z), \quad (2)$$

as a function of N . For all elements, $S(N)$ must lie along a straight line on a semilog plot when Eq. (1) accurately

describes the experimental data. The data points marked as “multifragmentation” in Fig. 1 show values of $S(N)$ extracted from isotope yields with $1 \leq Z \leq 8$ measured for multifragmentation events in central $^{124}\text{Sn} + ^{124}\text{Sn}$ and $^{112}\text{Sn} + ^{112}\text{Sn}$ collisions at $E/A = 50$ MeV [7]. Selection of central events ensures that the average excitation energies and temperatures in the participant source should be nearly identical [10]. The observed isoscaling is a necessary condition for the applicability of equilibrium models; such models have described other aspects of these collisions quite well [11].

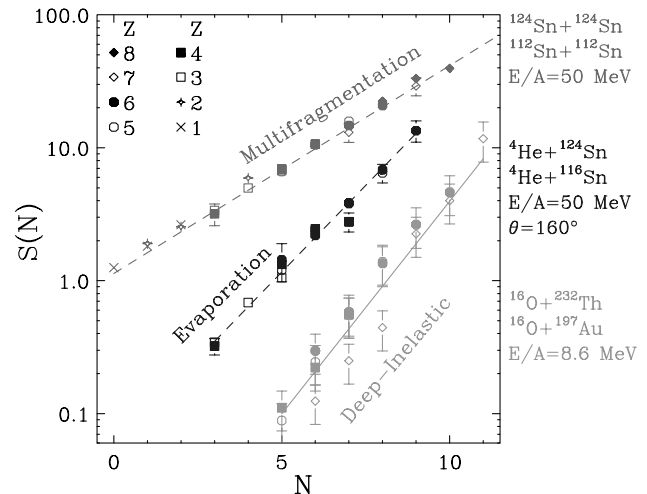


FIG. 1. The scaled isotopic ratio $S(N)$ is plotted as a function of the neutron number N , using the best fit value of β obtained from fitting isotopes with $Z \geq 3$. The data points plotted next to the label “multifragmentation” in Fig. 1 denote $S(N)$ extracted from multifragmentation events in central $^{124}\text{Sn} + ^{124}\text{Sn}$ and $^{112}\text{Sn} + ^{112}\text{Sn}$ collisions [7] with $\alpha = 0.37$, $\beta = -0.40$. The scaling behavior for evaporation process is illustrated by the reactions $^4\text{He} + ^{116}\text{Sn}$ and $^4\text{He} + ^{124}\text{Sn}$ [13] plotted next to the label “evaporation” with $\alpha = 0.60$, $\beta = -0.82$. Systematics of the strongly damped binary collisions is represented by the data of ^{16}O induced reactions on two targets ^{232}Th and ^{197}Au [12] plotted next to the label “deeply inelastic” with $\alpha = 0.74$, $\beta = -1.1$.

Rather surprisingly, isoscaling is also observed for strongly damped binary collisions (^{16}O induced reactions on two targets ^{232}Th and ^{197}Au) [12] and evaporative compound nuclear decay ($^4\text{He} + ^{116}\text{Sn}$ and $^4\text{He} + ^{124}\text{Sn}$ collisions) [13], for which grand-canonical ensemble approaches would appear to have little relevance. Our studies suggest that isoscaling is obeyed where (i) both reactions (1) and (2) are accurately described by statistical fragment emission mechanisms, and (ii) both systems are at nearly the same temperature. Indeed for deeply inelastic reactions emitted forward of the grazing angles ($^{22}\text{Ne} + ^{232}\text{Th}$ and $^{22}\text{Ne} + ^{97}\text{Zr}$ at $\theta = 12^\circ$ and $E/A = 7.9$ MeV [12]) and for reactions with different temperatures ($^{124}\text{Sn} + ^{124}\text{Sn}$ [7] and $^4\text{He} + ^{124}\text{Sn}$ [13]), isoscaling is violated. Conditions (i) and (ii) are met by the three reactions shown in Fig. 1. Why isoscaling is specifically observed in these cases and what aspects of statistical physics such scaling probes are examined below.

We first examine the strongly damped collisions, where isoscaling is reasonably well respected at low incident energies ($E/A < 10$ MeV) and at relatively backward angles [12,14], i.e., when equilibrium is established between the orbiting projectile and target. In such cases, the isotopic yields follow the “ Q_{gg} systematics” [12,14], and can be approximated by

$$Y(N, Z) \propto \exp[(M_P + M_T - M'_P - M'_T)/T], \quad (3)$$

where M_P and M_T are the initial projectile and target masses, and M'_P and M'_T are the final masses of the projectile- and target-like fragment. Here, T can be interpreted as the temperature. Equation (3) reproduces the systematics shown in Fig. 1. To show why this is so, we have expanded

$$dn(N, Z)/dt \propto T^2 \exp\{-V_c/T + Nf_n^*/T + Zf_p^*/T - [BE(N_i, Z_i) - BE(N_i - N, Z_i - Z) - BE(N, Z)]/T\}, \quad (5)$$

where V_c gives the Coulomb barrier, the terms f_n^* (f_p^*) represent the excitation contribution to the free energy per neutron (proton), BE is the binding energy, and N_i and Z_i identify the neutron and proton numbers of the parent nucleus.

Applying Eq. (5) to the calculations of R_{21} for two systems at the same temperature, we find that the binding energies of the emitted fragments cancel and the systematics shown in Fig. 1 can be reproduced. To understand why, we again expand the binding energy of the residue with neutron number $N_i - N$ and proton number $Z_i - Z$ to leading order in a Taylor series to obtain

$$R_{21}(N, Z) \propto \exp\{[(-\Delta s_n + \Delta f_n^*)N + [-\Delta s_p + \Delta f_p^* + e\Delta\Phi(Z_i - Z)]Z]/T\}, \quad (6)$$

where $\Phi(Z)$ is the electrostatic potential at the surface of a nucleus with neutron and proton number N and Z . Aside from the second order term from the electrostatic potential,

the nuclear binding energy contributions to the masses in Taylor series in N and Z . Expressing explicitly only the leading order terms that depend on N and Z , we obtain a relatively accurate leading order approximation to Eq. (3):

$$R_{21} \propto \exp[-(\Delta s_n N - \Delta s_p Z)/T], \quad (4)$$

where Δs_n and Δs_p are the differences of the neutron and proton separation energies for the two compound systems. Thus, the difference in the average separation energies in Eq. (4) plays a corresponding role to the difference in chemical potentials in the grand canonical approach, an intriguing result when one considers that $\mu \approx -s$ in the low temperature limit [15]. The straightforward dependence of Eq. (4) on temperature suggests that it may provide information relevant to the temperatures achieved in strongly damped collisions. The data of Fig. 1 imply a temperature of 2.7 MeV, not inconsistent with values derived from alternative analyses [12,14].

Next we consider the yields from processes involving the formation of a composite system and its subsequent decay via the evaporation of different isotopes. Corresponding scaled isotopic ratios for fragments detected at backward laboratory angles ($\theta = 160^\circ$) in $^4\text{He} + ^{116}\text{Sn}$ and $^4\text{He} + ^{124}\text{Sn}$ collisions at $E/A = 50$ MeV [13] are shown in Fig. 1, next to the label “evaporation.”

To explore the factors that govern the relevant evaporation rates, we utilize the formalism of Friedman and Lynch [16] which invokes statistical decay rates derived from detailed balance [17]. When the yields are dominated by emission within a particular window of source-mass or source-temperature, the relative yields of a fragment with neutron number N and proton number Z are directly related to the instantaneous rates

which is small for the decay of large nuclei, all factors in the exponent are proportional to either N or Z , consistent with Eq. (1). The corresponding scaling parameters α and β are functions of the separation energies, the Coulomb potential, and small contributions from the free excitation energies. Using the functions of Δs_n and Δf_n^* from Friedman and Lynch [16], one finds that a fixed temperature of about 3.7 MeV is required in Eq. (6) to obtain the experimental value of $\alpha = 0.6$. Running a full evaporation chain, using the procedure of Ref. [19], provides an average fragment emission temperature of about 3.3 MeV. These temperature values are comparable to those extracted by other techniques [13,18].

The expanding evaporating source (EES) model [19] provides an alternative description of multifragmentation. Within the context of that model, additional insights can be obtained. The EES model utilizes a formula for the particle emission rates which is formally identical to that of Eq. (5) but can differ significantly in its predictions because the residue may expand to subsaturation density

[20]. In this circumstance, the term enclosed in brackets “[]” containing three binding energies in Eq. (5) may vanish or become negative, enhancing the emission rate of fragments with $3 \leq Z \leq 20$. Detailed examination reveals that Δf_n^* in Eq. (6) is usually much smaller than Δs_n , and the volume, surface, and Coulomb contributions to Δs_n largely cancel, leaving the asymmetry energy term, $\text{Sym}(\rho) \times (N - Z)^2/A$, alone as the dominant contribution to α . For simplicity, we assume a power law dependence for $\text{Sym}(\rho)$, i.e., $\text{Sym}(\rho) = C_{\text{sym}} \times (\rho/\rho_0)^\gamma$ where γ is a variable and $C_{\text{sym}} = 23.4$ MeV is the conventional liquid drop model constant [21].

For illustration, we have performed calculations for the decay of the composite systems found in $^{124}\text{Sn} + ^{124}\text{Sn}$ and $^{112}\text{Sn} + ^{112}\text{Sn}$ collisions assuming, for simplicity, initial systems of $(Z_{\text{tot}}, A_{\text{tot}})$ of (100, 248) and (100, 224), respectively, initial thermal excitation energies of $E_{\text{ther}}^* = 9.5$ MeV, and initial collective radial expansion energies of $E_{\text{coll}}/A = 2.5$ MeV. The fragments are emitted from these systems as they expand from an initial density $\rho/\rho_0 = 1$ to $\rho/\rho_0 = 0.1$. The left panel of Fig. 2 shows two isoscaling functions, $S(N)$, calculated with the predicted isotope yields for $3 \leq Z \leq 6$ for $\gamma = 1$ and $\gamma = 0$. In spite of a rather complex interplay of expansion and fragment emission, the EES model predictions still exhibit an approximate scaling. Some of the calculated deviations from isoscaling may, in fact, be due to the rather schematic treatment of the Coulomb barrier penetration [22] and to the incomplete sequential decay information used in the model. Values for α , shown in the right panel, are determined from the slopes of the best fit of the lines to the predicted isoscaling functions.

For large values of γ , the asymmetry term, $C_{\text{sym}} \times (\rho/\rho_0)^\gamma$ decreases more rapidly with density and becomes

negligible as the residue expands. At low density where fragments are predominately emitted [19], the difference in isotopic yields from the two reactions 1 and 2 become smaller, resulting in flatter scaling functions and smaller values of α . [In the extreme case of identical yields from the two systems, $S(N)$ becomes a horizontal line corresponding to $\alpha = 0$.] The dot-dash line in the right panel of Fig. 2 joining the solid points shows the EES prediction that α decreases with increasing γ values. The multifragmentation data in Fig. 1 can be fairly well reproduced by $\gamma \approx 0.6$.

When the emission process ends at $\rho = 0.1\rho_0$, a low density residue (LDR) may remain. The final fate of this residue is not predicted by the EES model. A potential ambiguity may result if this residue is large and if its eventual disintegration produces a significant fraction of fragments with $Z \geq 3$. Calculations using the statistical multifragmentation model [23] with the mass and energy of the final LDR predict α values that increase with γ (dashed line)—opposite to the trend predicted for emission during the expansion. When γ decreases, the N/Z of the LDR from the two reactions, $^{124}\text{Sn} + ^{124}\text{Sn}$ and $^{112}\text{Sn} + ^{112}\text{Sn}$ become more similar, resulting in smaller α values—a trend also predicted from isospin dependent transport theory [24]. This accounts for the behavior of the dashed line in the right panel of Fig. 2. If high energy fragments are emitted primarily from the expanding system, and low-energy fragments come from the instantaneous disintegration of a low-density residue, then the results in Fig. 2 suggest that the predicted difference in the isoscaling for low and high energy fragments should be observable for $\gamma < 0.8$.

In summary, we have observed a scaling between isotopic distributions which allows a simple description of the dependence of such distributions on the overall isospin of the measured systems in terms of three parameters, α , β , and C . This scaling seems to apply to a broad range of statistical fragment production mechanisms, including evaporation, strongly damped binary collision, and multifragmentation. We have shown how this systematics arises within models frequently applied to such processes. In one such model, the EES model of multifragmentation, we find that the isoscaling parameters are sensitive to the density dependence of the asymmetry term of the EOS.

This work was supported by the National Science Foundation under Grants No. PHY-95-28844 and No. PHY-96-05140.

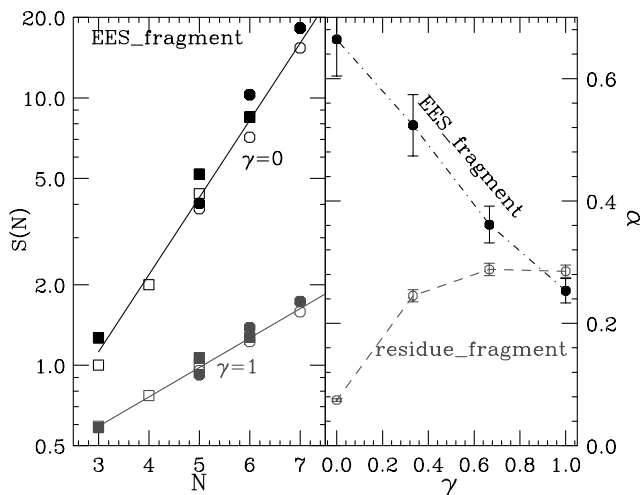


FIG. 2. Theoretical EES model predictions for the scaling functions $S(N)$ (left panel) and scaling parameter α (right panel) of fragments emitted in $^{124}\text{Sn} + ^{124}\text{Sn}$ and $^{112}\text{Sn} + ^{112}\text{Sn}$ collisions. The same convention as Fig. 1 applies to the various symbols used in the left-hand panel.

- [1] Bao-An Li *et al.*, Phys. Rev. Lett. **78**, 1644 (1997).
- [2] I. Bombaci *et al.*, Phys. Rep. **242**, 165 (1994).
- [3] J.M. Lattimer and M. Prakash, Astrophys. J. (to be published).
- [4] R. Laforest *et al.*, Phys. Rev. C **59**, 2567 (1999), and references therein.
- [5] R. Wada *et al.*, Phys. Rev. Lett. **58**, 1829 (1987).

- [6] W. U. Schroeder and U. J. Huizenga, *Treatise on Heavy Ion Science*, edited by D. A. Bromley (Plenum Press, New York, 1984), and references therein.
- [7] H. S. Xu *et al.*, Phys. Rev. Lett. **85**, 716 (2000).
- [8] J. Randrup and S. E. Koonin, Nucl. Phys. **A356**, 223 (1981).
- [9] S. Albergo *et al.*, Nuovo Cimento Soc. Ital. Fis. **89A**, 1 (1985).
- [10] G. J. Kunde *et al.*, Phys. Lett. B **416**, 56 (1998).
- [11] M. D'Agostino *et al.*, Phys. Lett. B **371**, 175 (1996); B. A. Li *et al.*, Phys. Lett. B **303**, 225 (1993); A. S. Botvina *et al.*, Nucl. Phys. **A584**, 737 (1995).
- [12] V. V. Volkov, Phys. Rep. **44**, 93 (1978).
- [13] J. Brzychczyk *et al.*, Phys. Rev. C **47**, 1553 (1993).
- [14] C. K. Gelbke *et al.*, Phys. Rep. **42**, 311 (1978).
- [15] S. R. Souza, W. P. Tan, R. Donangelo, C. K. Gelbke, W. G. Lynch, and M. B. Tsang, Phys. Rev. C **62**, 064607 (2000).
- [16] W. Friedman and W. Lynch, Phys. Rev. C **28**, 950 (1983).
- [17] This approach is similar to the Weisskopf model of V. Weisskopf, Phys. Rev. **52**, 295 (1937).
- [18] V. E. Viola, K. Kwiatkowski, and W. A. Friedman, Phys. Rev. C **59**, 2660 (1999).
- [19] W. A. Friedman, Phys. Rev. Lett. **60**, 2125 (1988); Phys. Rev. C **42**, 667 (1990).
- [20] Note: $f^*(T/\epsilon_f)/T$ remains roughly constant during expansion.
- [21] Aage Bohr and Ben R. Mottelson, *Nuclear Structure* (W. A. Benjamin, Inc., New York, 1998), Vol. II.
- [22] J. Töke, W. Gawlikowicz, and W. U. Schröder, Phys. Rev. C **63**, 024606 (2001).
- [23] A. Majumder and S. Das Gupta, Phys. Rev. C **61**, 034603 (2000); Scott Pratt and Subal Das Gupta, Phys. Rev. C **62**, 044603 (2000).
- [24] W. Tan *et al.*, NSCL report No. MSUCL-1198 (2001).